Crystal nucleation in the one-component plasma

Jérôme Daligault*
Theoretical Division, Los Alamos National Laboratory, Los Alamos, New Mexico 87545, USA
(Received 26 January 2006; revised manuscript received 3 April 2006; published 30 May 2006)

We have performed molecular dynamics simulations to study the kinetics of crystal nucleation in the one-component plasma. We have monitored nucleation in the supercooled liquid phase by following the time evolution of the size distribution of crystal nuclei formed during the phase transition. Although several observations are consistent with classical nucleation theory such as transient effects and the existence of a free-energy barrier to crystallization, we could not unambiguously identify a critical size for the crystal nuclei formed within the metastable phase.

DOI: 10.1103/PhysRevE.73.056407 PACS number(s): 52.27.Gr

I. INTRODUCTION

It is remarkable that systems of charged particles interacting via a purely repulsive (pure or screened Coulomb) interaction can crystallize, i.e., can spontaneously self-assemble into macroscopic periodic lattice structures when the mean potential energy greatly dominates the mean kinetic energy. Wigner noted long ago that the electron gas forms a crystal at low enough density, and two-dimensional electron crystals have since been observed [1]. Wigner crystals are not mere curiosities but are now observed in diverse systems such as dusty plasmas [2], and charged colloids [3], laser-cooled trapped ions [4], and are predicted to be possible in ultracold plasmas [5]. Interestingly, colloids and dusty plasmas are currently used to shed new light on the freezing transition; they are indeed easily visualized and their kinetics can be resolved, because of the long time scales associated with mesoscopic particles. Wigner crystallization plays also an important role in astrophysics. For instance, the cooling evolution of white dwarfs and neutron stars is significantly affected by the crystallization of their interiors and crusts, respectively, composed of mixtures of bare nuclei moving in a nearly homogeneous electron background.

It is fair to say, however, that the crystallization phenomenon in Coulomb systems is not well understood. This is particularly true for the two reference models, namely, the one-component plasma (OCP) and the Yukawa OCP, used to understand the properties of more realistic systems. The OCP consists of a single species of charged particles immersed in a uniform, neutralizing background; it is characterized at temperature T and density ρ by the coupling parameter $\Gamma = q^2/a\,k_B T$, where $a=(3/4\pi\rho)^{1/3}$ is the mean interparticle distance and q the particles' charge. In the Yukawa OCP, particles interact through an exponentially screened Coulomb potential. Although studied in great detail in the past, much of the progress in understanding freezing in these systems has involved equilibrium aspects: the phase diagram, entropy, and energy changes at freezing [6,7], and quantum effects [8]. For instance, increasingly accurate Monte Carlo (MC) calculations have pinpointed the liquid-solid transition of the classical OCP at $\Gamma_m \simeq 175$ with the bcc lattice having the lowest possible free energy, followed closely by the fcc lattice.

The objective of the present study is to investigate dynamic aspects of the crystallization in the classical OCP. We shall focus on crystal nucleation, i.e., the process by which a (supercooled) liquid starts to phase separate by forming small, localized crystal nuclei within the metastable phase. We have investigated the kinetics of nucleation using molecular dynamics (MD) simulations over a wide range of undercooling, $\Gamma_m \leq \Gamma \leq 2000$. The particle-particle particle-mesh algorithm was used to deal with the long-range Coulomb interaction and allowed us to perform highly accurate simulations over reasonable computational times of large systems ($N=16\,000$) over long periods of time ($t_{sim} > 70\,000$ in units of the inverse plasma frequency ω_p). We have monitored nucleation by following the time evolution of the excess energy, the pair distribution function, and, most importantly, the size distribution of crystal nuclei. We have analyzed the observations on the basis of classical nucleation theory (CNT) [9], whose basic assumptions are critically reviewed. The salient results of this study are, first, an unequivocal demonstration of the occurrence of nucleation. Second, for any particular nucleation event, the kinetics seem to be qualitatively in accord with the predictions of CNT: existence of a transient regime and dependence upon Γ of the kinetics. However, assuming that CNT assumptions are sound, we could not unambiguously identify a critical size for the crystal nuclei formed within the metastable phase, beyond which they grow spontaneously.

II. EVIDENCE OF CRYSTALLIZATION AND GENERAL OBSERVATIONS

The method of MD has yielded much insight into the nature of homogeneous crystal nucleation of systems interacting via simple, short-ranged potentials [10,11]. Hammerberg *et al.* reported evidence of crystallization in the Yukawa OCP using truncated potentials and large screening lengths [12]. As for the OCP, to our knowledge, only two independent works based on MC simulations reported the crystallization from the melt [13,14]. The method of MD has the advantage of giving access to the actual kinetics of the phase transition. Note that MD was recently used to look at

*Electronic address: daligault@lanl.gov

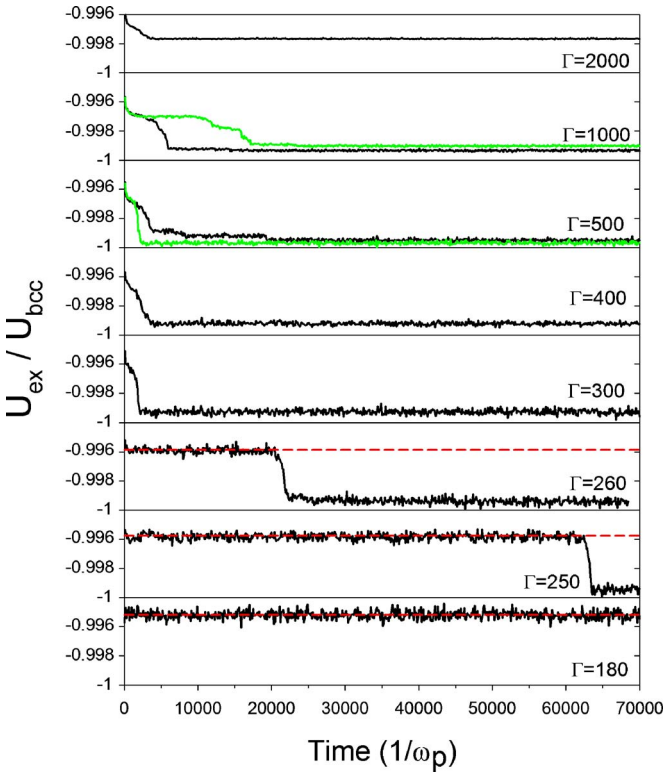

FIG. 1. (Color online) Evolution of the excess energy for different values of Γ (U_{ex} is normalized to the absolute value of the bcc lattice excess energy U_{bcc}). The dashed lines are the thermodynamic excess energy of [6]. Two simulations at $\Gamma=500,1000$ are shown. Here $N=1024$.

size effects in melting of the OCP, the opposite side of the coin from crystallization [15].

We employed a Nosé-Hoover thermostat to maintain the system at constant temperature (N,V,T ensemble). The time step is $\delta t=0.01/\omega_p$, which ensures good (Nosé-Hoover) energy conservation ($\Delta E/E\sim 10^{-6}$). We performed "instantaneous" quenches in the range $\Gamma_m\leq\Gamma\leq 2000$, i.e., starting from an initial random particle configuration at $\Gamma\geq\Gamma_m$, the system then evolves freely at this value; to improve the statistics, different initial configurations were also used. Figure 1 shows, for a sample of simulations, the time evolution of the instantaneous excess energy $U_{ex}(t)$. In the N,V,T ensemble, the onset of crystallization is marked by the decrease in the pressure P, or equivalently in U_{ex} since $U_{ex}=3(PV-Nk_BT)$ (V=volume). Crystallization is also evidenced by the pair distribution functions as shown in Fig. 2. In the range $\Gamma_m\leq\Gamma<250$, simulations showed no indication of freezing over the simulation length t_{sim}. The system settles into a supercooled liquid state, whose average excess energy reproduces to excellent accuracy the MC data of DeWitt *et al.* [6]. The large degree of observed undercooling without crystallization demonstrates the existence of a kinetic barrier to the transformation. The route found by the system to overcome that barrier and reach the minimum of the free energy involves nucleation followed by growth and coalescence of crystal nuclei. The rate at which the nuclei form is extraordinarily sensitive to the extent of penetration into the supercooled region, and our results suggest that rate is certainly very small near $\Gamma=\Gamma_m$. This makes simulating the crystallization process right above Γ_m challenging since the liquid phase remains metastable for a period of time much longer than achievable simulation times t_{sim}. At large enough undercooling, $\Gamma\geq 250$, the nucleation rate is small enough to make nucleation occurring over t_{sim}: crystal nuclei form and U_{ex} drops rapidly to a value slightly larger than the excess energy U_{bcc} of the bcc lattice. We always observed crystallization when $250\leq\Gamma\leq 1000$ and the final configuration is almost always an imperfect bcc crystal with a variety of lattice defects (see Fig. 2); only one simulation at $\Gamma=1000$ ended with an imperfect fcc lattice. Figure 1 also reveals a strong dependence of $U_{ex}(t)$ upon Γ and the initial configuration. Below $\Gamma=300$, the system remains in a supercooled liquid state for some period of time, which decreases with Γ. When $300\leq\Gamma\leq 1000$, no such transient regime is observed and $U_{ex}(t)$ drops rapidly to its final value over a time that tends to increase with $\Gamma>400$. At very high undercooling $\Gamma=2000$, we did not observe crystallization and the system stayed in a metastable state. It is worth noting that our results corroborate the MC results of DeWitt *et al.* [13].

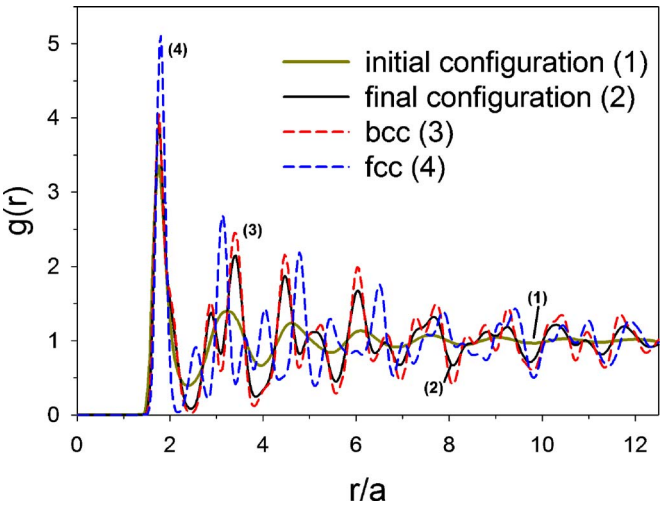

FIG. 2. (Color online) Comparison of the final pair distribution function $g(r)$ in a simulation at $\Gamma=400$ ($N=4394$) with the bcc and fcc $g(r)$ at $\Gamma=400$.

III. FINITE-SIZE EFFECTS

A major question is whether the periodic boundary conditions affect the nucleation. Because nucleation rate in a bulk sample is proportional to its volume, the simulated nucleation rate should be proportional to N if the nucleation is truly homogeneous. In [16], the authors found (with Lennard-Jones systems) that the nucleation rate decreased with N from 108 to 1500, showing that the nucleation must have been induced by the periodic boundary conditions. Later, MD results for Lennard-Jones systems using up to 10^6 particles suggested that by 15 000 particles the effects of system size dependence had disappeared, but that the million-particle system was necessary to exhibit the full diversity in nucleation behavior of a macroscopic system [10].

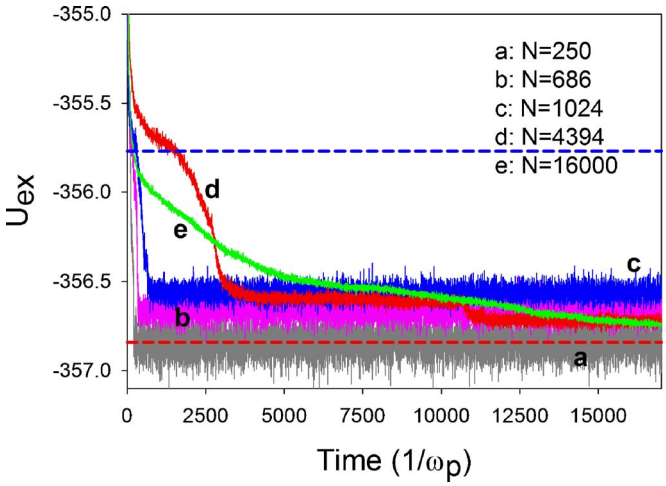

FIG. 3. (Color online) Dependence upon N of $U_{ex}(t)$ at $\Gamma=400$. Dashed lines: excess energy of [6] for the liquid and bcc lattice.

Figure 3 shows the evolution of U_{ex} for $\Gamma=400$ and N varying from 250 to 16 000 particles. In all cases, U_{ex} starts dropping to its final value just after the simulation begins. The initial decay rate, however, decreases with N from 250 to 4396, and is larger with $N=16\,000$ than with $N=4394$, which is reminiscent of the above mentioned size effect observed in [16]. Moreover, for $N=16\,000$, U_{ex} decreases steadily, suggesting that the so-called catastrophic growth observed at smaller N is certainly another size effect. We shall mention later that the final distributions of nuclei are essentially independent of N. We also note that the choice of N at a bcc ($N=2n^2$), fcc ($N=4n^3$), or any other number appears to bear no essential consequences to the solidification process. All the conclusions drawn in this paper are based on simulations with 4374 and 16 000 particles, for which size effects become negligible, at least during the initial nucleation dynamics. The subsequent coalescence of crystal nuclei is certainly affected by size effects.

IV. THE NUCLEATION DYNAMICS

In order to extract detailed information on the nucleation dynamics itself, it is essential to identify and monitor the time evolution of crystal nuclei, which is by no means straightforward. We used two distinct methods, the Voronoi polyhedron analysis and the local bond-order parameter analysis (see the Appendix). Both methods consist of examining the local coordination about particles, which, because it differs between liquid and crystal, allows one to distinguish "liquid" particles from "solid" particles. Crystal nuclei are then identified by counting the connections between the solidlike particles. As illustrated in the Appendix, both methods agree very well with one another, thereby ensuring the reliability of our identification procedure and of the analysis discussed in the following. In the following, at any time t, $N(p,t)$ denotes the number of nuclei of size $p \geq 1$, $N_{nuc}(t) = \Sigma_{p\geq 1} N(p,t)$ the total number of nuclei, $N_s(t) = \Sigma_{p\geq 1} pN(p,t)$ the total number of solid particles, $N_p = \Sigma_{p'>p} N(p',t)$ the number of nuclei of size larger than p, and $p^*(t)$ the size of the largest nucleus. Figure 4 illustrates the typical evolution of N_{nuc}, N_s, p^*, and N_p with p from 10 to 40 for a simulation at $\Gamma=400$ and $N=4394$. Similar evolutions were obtained with other Γ values, and the following discussion is based upon all the cases studied. Initially, there are no crystal nuclei in the supercooled liquid. Eventually a few solid particles appear, and small nuclei form and grow (note the correlation between crystal nuclei growth and the decay of U_{ex}, Fig. 3). Eventually, the different quantities stop increasing and fluctuate around a nearly constant mean value until the end of the simulation. This sudden change occurs probably because of the significant depletion of liquidlike particles. The final system is a mosaic of large nuclei separated by liquid particles and small nuclei that attach and detach to the existing nuclei without effectively creating new large ones. Moreover the diffusion coefficient is very small but finite. Other general observations are worth noting. The final ratio N_s/N varies with Γ, N (>500), and the initial configuration in a relatively wide range, $N_s/N \simeq 0.6-0.9$. However, independently of Γ and N, the average number of particles per nucleus N_{nuc}/N_s reaches the value ~ 10, and p^* fluctuates with time around the value $p^* \simeq 40$ particles.

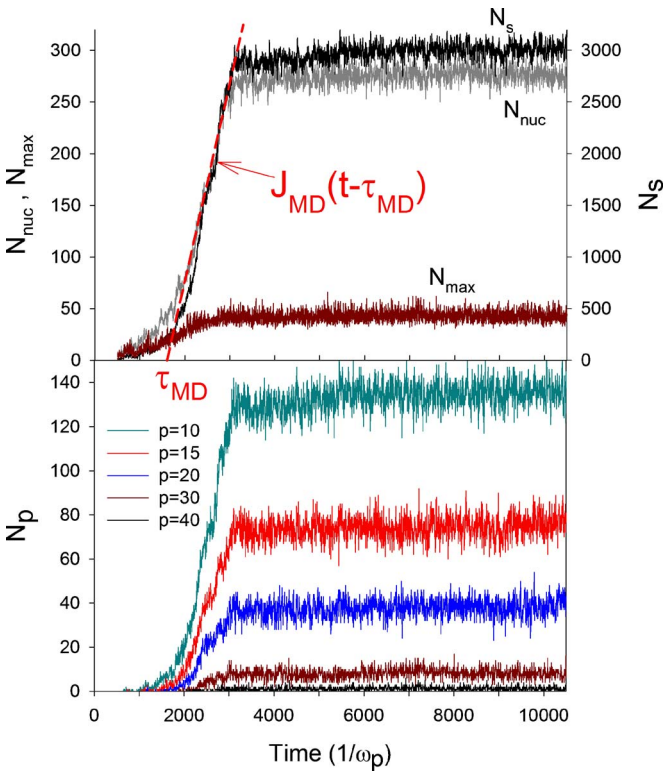

FIG. 4. (Color online) Time evolution of N_{nuc}, p^*, N_s (right axis), and N_p (from top to bottom $p=10,15,20,30,40$) in a simulation at $\Gamma=400$ and $N=4394$. See also Fig. 9 for results with $\Gamma=300$ and $N=4394$.

During the nucleation phase, N_{nuc} and N_s first grow nonlinearly but then grow nearly linearly, e.g., $N_{nuc}(t) \simeq J_{MD}(t-\tau_{MD})$, $t > \tau_{MD}$ (see Fig. 4) where both J_{MD} and τ_{MD} obviously depend on Γ. Such behavior can be understood qualitatively on the basis of CNT. CNT is a phenomenological theory that involves a set of coupled rate equations for the number density $N(p,t)/V$ by which crystal nuclei grow or

shrink via the attachment or loss of single particles. In its most common formulation, CNT assumes that a steady state is rapidly established such that the rates at which nuclei of size i grow to size $i+1$ are constant (denoted J_0) and independent of time and p. The steady state approximation was used, for instance, in [12] to interpret MD simulations of the Yukawa OCP, in [17] as a model of crystallization in neutron stars, and in [18] to predict the glass transition in the OCP. This approximation leads to the linear relation $N_{nuc}(t)/V = \int_0^t J_0 dt = J_0 t$, which contrasts with our observations. It is therefore important to take account of transient nucleation behavior in interpreting crystallization kinetics, which challenges the conclusions of the above-cited works [12,17,18]. When transient effects are considered, CNT predicts a time-dependent nucleation rate $J(t)=J_0[1-\exp(-t/\tau)]$, where τ is an effective time lag. The nucleation rate is initially low and increases to a steady state value J_0, over a transient time $\simeq\tau$. At large time, $N_{nuc}\simeq J_0(t-\tau)$, in agreement with our results if one assumes $J_0=J_{MD}$ and $\tau=\tau_{MD}$; the overall MD nucleation rate, however, is not well reproduced by $J(t)$.

According to CNT, J_0 and τ result from the competition of a thermodynamic factor proportional to $\exp(-\Delta F^*/k_BT)$ and a kinetic factor proportional to $\exp(-\Delta E/k_BT)$. The former reflects that nucleation is an activated process; a free-energy barrier $\Delta F^*=16\pi\sigma^3/3\Delta f^2$ must be overcome in order to form (spherical) nuclei of a critical size p_c, from which the stable phase will grow; here Δf is the difference in (Helmoltz) free energies between the solid and liquid phases and σ is the surface energy density. The kinetic factor describes the rate of attachment of particles to a critical nucleus. Liquid particles are assumed to diffuse until they "jump" from the liquid to the solid phase, by overcoming the same activation barrier ΔE as in the liquid; for the OCP, we recently evaluated $\Delta E/k_BT=0.008\Gamma$ [19]. In order to see how J_0 and τ vary with Γ, we evaluated Δf using the results of [6] and assumed the hard-sphere result $\sigma\propto k_BT/a^2$ [20]. The results (not shown here) reproduce only qualitatively the variations with Γ of J_{MD} and τ_{MD}. The nucleation rate varies by orders of magnitude because of the exponentiations and goes through a maximum at Γ_c, when Γ is increased above Γ_m [9]; τ reaches a minimum at Γ_c and p_c decreases from a few hundreds near Γ_m to less than one at high enough Γ. These variations explains why nucleation appears as a sudden phenomenon when the liquid OCP is deeply undercooled to $\Gamma \geq 300$. A rigorous comparison, however, is difficult; for instance, one could not use the expression for J_0 to calculate the surface energy σ (the only unknown parameter) from the measured J_{MD}. In fact, we could not clearly recognize, in each run, when the nuclei become of critical size. In all cases, N_{nuc} starts its quick rise when $p\simeq 20-25$ particles, independently of Γ. Therefore, if the concept of a critical size is correct, this size is certainly very small, $p_c\sim 20-25$ (for $\Gamma>250$) but is nevertheless larger than the 14 nearest neighbors in a bcc lattice. Note that here surface particles are counted in p_c (see the Appendix).

Other assumptions underlying CNT are also questionable. The nuclei present a wide range of morphologies and can not be regarded as spherical as supposed in CNT. Moreover, in CNT, nuclei grow or shrink via the attachment or loss of single molecules. Detailed analysis revealed, however, that many of nuclei and liquid particles collide and fuse for some period of time and may fission into two or more other nuclei. It is also possible that the proper description of nucleation should involve collective modes, predominant in the OCP; local fluctuations could indeed lead to the sudden appearance of crystal nuclei elsewhere.

V. SUMMARY

We have studied the onset of crystallization of a supercooled one-component plasma with MD simulations. We have analyzed the results on the basis of CNT. We have pointed out the importance of considering the transient period, especially near Γ_m. The variations with Γ and the nucleation kinetics are consistent with CNT. We could not, however, identify unambiguously a critical nucleus size. Further studies and better statistics should allow us to test CNT in more detail and to study the effect of collective modes alluded before. Such a thorough study with molecular dynamics would certainly benefit from sophisticated Monte Carlo simulations to estimate key quantities in CNT such as ΔF^*, p_c, and the kinetic prefactor [21]. This work could be extended to investigate the crystallization kinetics in Coulomb mixtures and the effect of impurities on nucleation, as encountered in astrophysical objects.

ACKNOWLEDGMENTS

The author wishes to thank Hugh E. DeWitt for his interest, helpful discussions, and continuing encouragement. This research is supported by the Department of Energy, under Contract No. W-7405-ENG-36.

APPENDIX: VORONOI POLYHEDRON AND LOCAL BOND-ORDER PARAMETER ANALYSIS

The unequivocal identification of a crystal nucleus in a molecular dynamics simulation is difficult. We used two distinct methods, the (modified) Voronoi polyhedron analysis and the local bond-order analysis. For more details on the Voronoi polyhedron analysis, see [10,22,23]. For more details on the local bond-order parameter analysis, see [21].

Voronoi polyhedron analysis

The Voronoi polyhedron associated with a given particle is defined as the set of all points of space that are closer to that particle than to any of the others. In a perfect crystal, the Voronoi polyhedron reduces to the Wigner-Seitz cell. The shape of a Voronoi polyhedron is an indication of the nearest-neighbor environment of a particle, and can be used to classify the coordination of each particle as being either bcc, fcc, or otherwise. Following [22], the signature of a λ-faced Voronoi polyhedron is defined by a set of integers $(n_3,n_4,\ldots)$, where n_l is the number of l-sided faces of the polyhedron, and $\lambda=\Sigma_{l\geq 3}n_l$. For example, the Voronoi polyhedron of a particle in a perfect bcc lattice is a truncated octahedron that has six square-shaped and eight hexagonal-shaped faces, and its signature is $(0,6,0,8,\ldots)$. The Voronoi

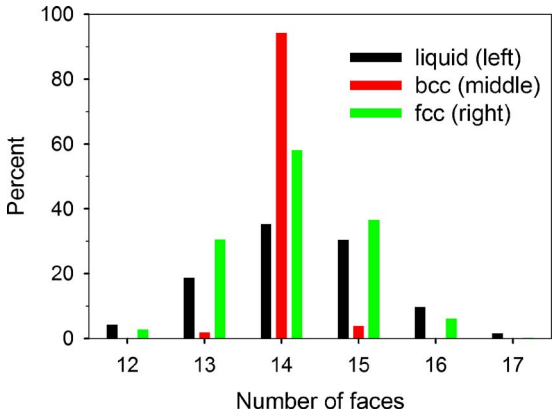

FIG. 5. (Color online) Histograms from MD simulations of the number of faces of Voronoi polyhedra in an OCP at $\Gamma=260$ in the supercooled liquid state (i.e., before nucleation), the bcc phase, and the fcc phase.

polyhedron of a particle in a perfect fcc structure is a rhombic dodecahedron that has 12 lozenge-shaped faces, and its signature is $(0,12,0,0,\ldots)$. As illustrated in Figs. 5 and 6, in a physical system, the thermal motions of the particles affect significantly the distribution of signatures of the Voronoi polyhedra. For instance, the characteristic Voronoi polyhedron associated with the fcc lattice is affected by the smallest perturbations of the particle positions from their positions in a perfect lattice. The reason for that is that of the 14 vertices of the rhombic dodecahedron there are six where four faces meet. Any thermal motion destroys these fourfold vertices, which break up into sets of threefold vertices connected by short edges. The result is that a variety of polyhedra with signatures $(0,4,4,6,\ldots)$, $(0,3,6,5,0,\ldots)$, $(0,3,6,4,0,\ldots)$,$(0,4,4,7,0,\ldots)$,… occur in a thermally

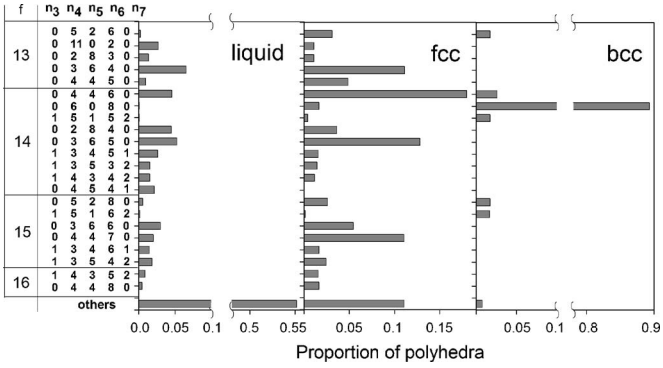

FIG. 6. Histograms from MD simulations of the distribution of signatures of Voronoi polyhedra for the OCP at $\Gamma=260$ in the supercooled liquid phase (before nucleation), the bcc phase, and the fcc phase. We only show the signatures whose proportion is larger than 1.5%; all the other signatures are gathered in the bottom bar labeled "others." The perfect bcc and fcc signatures are $(0,6,0,8,\ldots)$ and $(0,12,0,0,\ldots)$, respectively. We note that the $(0,12,0,0,\ldots)$ signature does not appear in the histogram for fcc. Indeed thermal distortions destroy the fourfold vertices of the rhombic dodecahedron, which results in a variety of polyhedra that have threefold vertices only. The bcc polyhedron is much more stable as evidenced by the large proportion of $(0,6,0,8,\ldots)$ signatures.

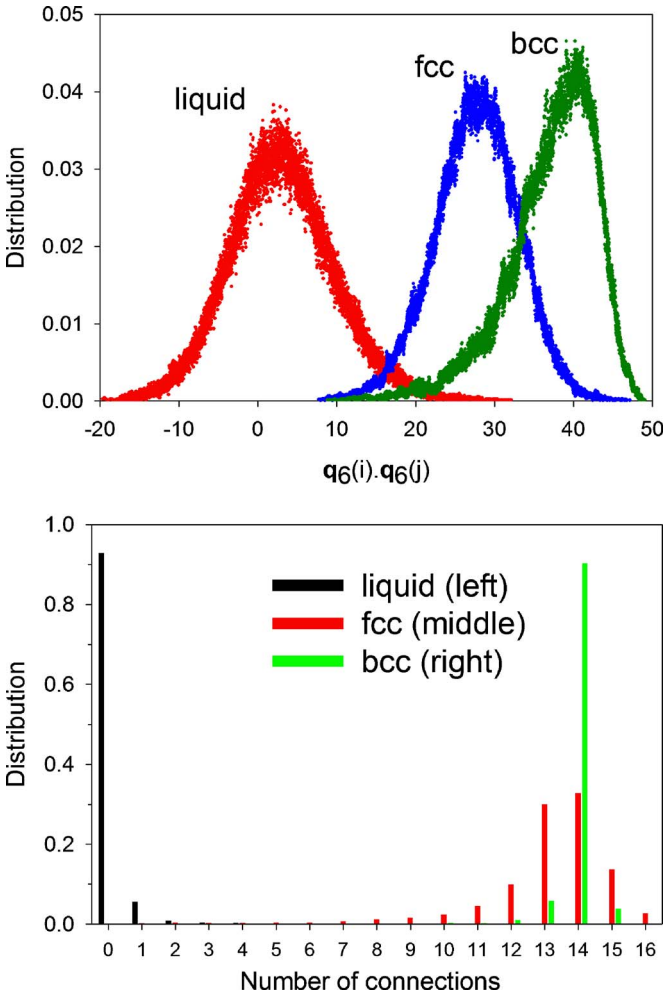

FIG. 7. (Color online) (upper panel) Histograms from MD simulations of the dot product $\mathbf{q}_6(i)\cdot\mathbf{q}_6(j)$ in an OCP at $\Gamma=260$ in the supercooled liquid state, the bcc phase, and the fcc phase. In each case, the distribution function is the superposition of 100 histograms obtained for 100 configurations separated in time by $2/\omega_p$ along the system trajectory. (Lower panel) Histograms of the number of connections per particle in an OCP at $\Gamma=260$. In each case, the histogram was obtained by averaging over the 100 configurations shown in the upper panel.

equilibrated fcc crystal. The bcc Voronoi polyhedron, with only threefold vertices, is much more stable against thermal distortions, although the number of different signatures increases as one approaches to the liquid-solid transition line. In order to cope with the effect of thermal fluctuations and to identify fcc crystalline regions, we used the modified Voronoi polyhedron analysis advocated in [10]. For each particle configuration sampled along the trajectory, the modified analysis consists of a short steepest-descent energy minization toward an inherent structure followed by a Voronoi polyhedron analysis of the latter.

The Voronoi analysis provides a convenient definition of neighboring particles. If the Voronoi polyhedra associated with two particles have a face in common, we say the two particles are neighbors. For instance each particle of a perfect bcc lattice has 14 neighbors, while a particle in a perfect fcc lattice has 12 neighbors. This definition of neighbors allows

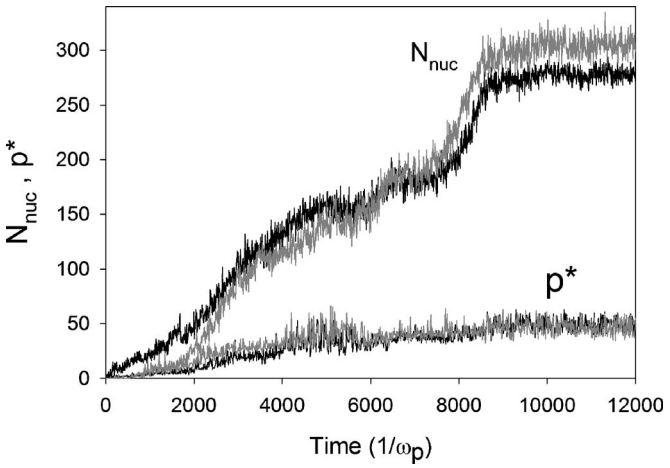

FIG. 8. Comparison between the total number of nuclei N_{nuc} and the largest nucleus size p^* as obtained with the Voronoi polyhedron analysis (black lines) and with the local bond-order parameter analysis (gray lines). Here $\Gamma=300$ and $N=4394$.

us to identify solid nuclei. For instance, we say that any two particles that are in a bcc environment, i.e., the signature of their Voronoi polyhedron is $(0,6,0,8,\ldots)$ for both particles, and are also neighbors are part of the same solid nucleus.

Local bond-order parameter analysis

For the identification of solidlike particles, we seek to define a criterion that allows us to distinguish between the liquid on the one hand, and all possible solid structures on the other. Frenkel and collaborators defined such a criterion based on local bond-order parameters, which provide a measure of the local structure around a particle (see Ref. [21] for details). The authors successfully applied this criterion to Lennard-Jones and hard-sphere systems. We show below that this criterion applies also to OCP systems. For a particle labeled i, we define a $[(2\times 6)+1]$-dimensional complex vector $\mathbf{q}_6(i)$ with the components

$$q_{6m}(i) = \frac{1}{N_b(i)} \sum_{j=1}^{N_b(i)} Y_{6m}(\hat{\mathbf{r}}_{ij})$$

where $m=-6,\ldots,6$, the sum goes over all neighboring particles $N_b(i)$ of particle i, and $Y_{6m}(\hat{\mathbf{r}}_{ij})$ are the spherical harmonics evaluated for the normalized direction vector $\hat{\mathbf{r}}_{ij}$ between particle i and its neighbor j. Neighbors are defined as before: two particles are neighbors if their Voronoi polyhedra have a face in common. We also define a dot product of the vectors $\mathbf{q}_6$ of neighboring particles i and j,

$$\mathbf{q}_6(i)\cdot\mathbf{q}_6(j) \equiv \sum_{m=-6}^{6} q^*_{6m}(i) q_{6m}(j),$$

where the asterisk indicates the complex conjugate. In simple liquids we expect that there is no preferred orientation around a particle and, therefore, we expect the degree of orientational correlations $\mathbf{q}_6(i)\cdot\mathbf{q}_6(j)$ of the vectors $\mathbf{q}_6(i)$ and $\mathbf{q}_6(j)$ to be small. In contrast, for a particle with a crystal-

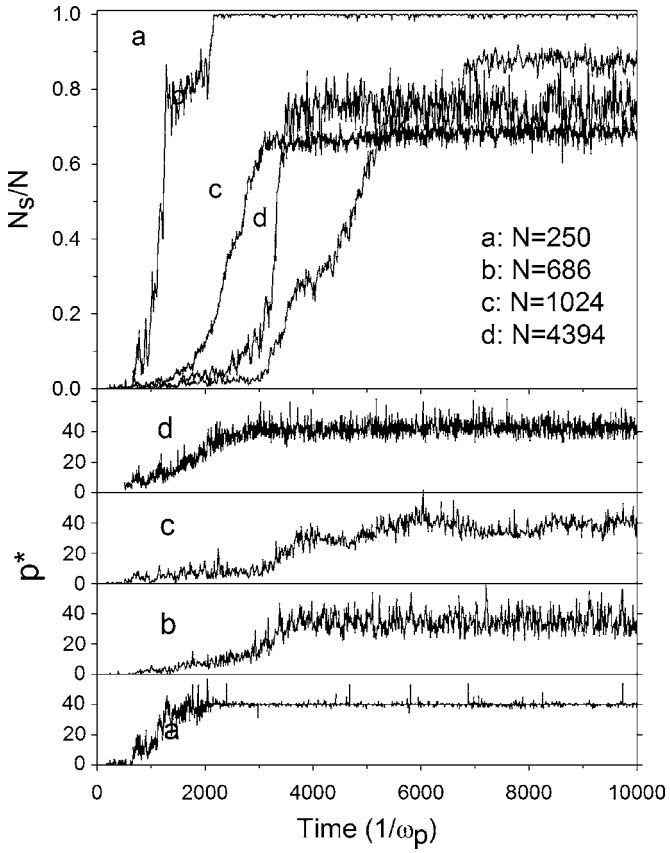

FIG. 9. Evolution of the ratio N_s/N and p^* for different total number of particles N for an OCP with $\Gamma=400$.

linelike environment the vector orientations are correlated and we expect $\mathbf{q}_6(i)\cdot\mathbf{q}_6(j)$ to be much larger. In Fig. 7, we show histograms of the dot product $\mathbf{q}_6(i)\cdot\mathbf{q}_6(j)$ of the OCP at $\Gamma=260$ in the liquid state, the bcc phase, and the fcc phase. The relevant solid structures, which for the OCP system are bcc and fcc, yield much higher values for the dot product than the liquid. Two neighboring particles i and j are then said to be connected if the dot product $\mathbf{q}_6(i)\cdot\mathbf{q}_6(j)$ exceeds a certain threshold; in this paper we chose a threshold value equal to 20. We show in Fig. 7 the histograms for the number of connections per particles in a liquid OCP as well as in a bcc and fcc OCP at $\Gamma=260$. The number of connections is much smaller for a particle in a liquid than in a solid. The peak for the bcc structure is at 14, which corresponds exactly to the number of nearest neighbors in a perfect lattice. For the fcc structure, the peak is shifted to higher values (around 13–14) with respect to the number of nearest neighbors in a perfect fcc lattice (12), which indicates that at $\Gamma=260$ the fcc structure is relatively more disordered than the bcc structure (recall that the fcc free energy is higher than for the bcc); the OCP fcc structure is strongly affected by thermal fluctuations. In order to unambiguously distinguish between liquidlike and solidlike particles, we impose a threshold on the number of connections a particle has with its neighbors. All particles with less (more) connections than this threshold are considered to be liquid-like (solidlike). We should keep in mind that, in a small nucleus, most particles are at the surface and that they should be considered as solidlike. We

found that this is achieved if we choose threshold value between 6 and 8; the results shown in this paper were obtained with a threshold value equal to 7. Now that we have a criterion to distinguish between liquidlike and solidlike particles, we can define solid nuclei as follows: a solid nucleus is a set of solidlike particles that are connected. Note that here no distinction is made between different crystal structures. Moreover, whereas the number of particles depends somewhat on the choice of the threshold values, the conclusions drawn in our present study are insensitive to the threshold values used.

Comparison between the two analyses

In Fig. 8 we compare the results obtained with the two methods for an OCP at $\Gamma=300$ and $N=4394$. As mentioned in the paper, both methods yield results in very good agreement with each other and our conclusions are independent of the analysis used. We note that the total number of nuclei obtained with the local bond-order parameter analysis is alternatively smaller at shorter times and larger at larger times than the number obtained with the Voronoi polyhedron analysis; the same trend was noticed for all the Γ values we looked at. The Voronoi polyhedron analysis therefore tends to lead to a critical size p_c slightly larger to the one found with the other analysis technique.

Size effects

Finally, for completeness, Fig. 9 compares the variation of N_s/N and p^* obtained with MD for different number of particles N.

[1] E. Wigner, Phys. Rev. **46**, 1002 (1934); C. C. Grimes and G. Adams, Phys. Rev. Lett. **42**, 795 (1979).

[2] H. Thomas, G. E. Morfill, V. Demmel, J. Goree, B. Feuerbacher, and D. Mohlmann, Phys. Rev. Lett. **73**, 652 (1994); J. H. Chu and L. I, *ibid.* **72**, 4009 (1994); Y. Hayashi, *ibid.* **83**, 4764 (1999).

[3] T. Palberg, J. Phys.: Condens. Matter **11**, R323 (1999).

[4] W. M. Itano *et al.*, Science **279**, 686 (1998).

[5] T. Pohl, T. Pattard, and J. M. Rost, Phys. Rev. Lett. **92**, 155003 (2004); T. C. Killian, Nature (London) **429**, 815 (2004).

[6] H. DeWitt and W. Slattery, Contrib. Plasma Phys. **39**, 97 (1999).

[7] S. Hamaguchi, R. T. Farouki, and D. H. E. Dubin, Phys. Rev. E **56**, 4671 (1997).

[8] M. D. Jones and D. M. Ceperley, Phys. Rev. Lett. **76**, 4572 (1996).

[9] K. F. Kelton, in *Solid State Physics*, edited by H. Ehrenreich and D. Turnbull (Academic, Boston, 1991), Vol. 45, p. 75.

[10] W. C. Swope and H. C. Andersen, Phys. Rev. B **41**, 7042 (1990), and references therein.

[11] B. O'Malley and I. Snook, Phys. Rev. Lett. **90**, 085702 (2003).

[12] J. E. Hammerberg, B. L. Holian, and R. Ravelo, Phys. Rev. E **50**, 1372 (1994).

[13] H. E. DeWitt *et al.*, in *Proceedings of the International Conference on the Physics of Strongly Coupled Plasmas*, edited by H. M. Van Horn and S. Ichimaru (University of Rochester Press, Rochester, NY, 1993).

[14] S. Ogata, Phys. Rev. A **45**, 1122 (1992).

[15] J. P. Schiffer, Phys. Rev. Lett. **88**, 205003 (2002).

[16] J. D. Honeycutt and H. C. Andersen, Chem. Phys. Lett. **108**, 535 (1984); J. Phys. Chem. **90**, 1585 (1986).

[17] F. V. De Blasio, Astrophys. J. **452**, 359 (1995).

[18] S. Tanaka and S. Ichimaru, Phys. Rev. A **35**, 4743 (1987).

[19] J. Daligault, Phys. Rev. Lett. **96**, 065003 (2006).

[20] D. W. R. Marr, J. Chem. Phys. **102**, 8283 (1995).

[21] P. Rein ten Wolde *et al.*, J. Chem. Phys. **104**, 9932 (1996); S. Auer and D. Frenkel, Adv. Polym. Sci. **173**, 149 (2005).

[22] M. Tanemura *et al.*, Prog. Theor. Phys. **58**, 1079 (1977).

[23] C. S. Hsu and A. Rahman, J. Chem. Phys. **71**, 4974 (1979).